Design and modeling of tapered waveguide for photonic crystal slab coupling by using time-domain Hertzian potentials formulation

A. Massaro, M. Grande, R. Cingolani, A. Passaseo, M. De Vittorio

National Nanotechnology Laboratory of CNR-INFM , Distretto Tecnologico-ISUFI, Università di Lecce, Via Arnesano,73100 Lecce, Italy.
alessandro.massaro@unile.it

Abstract: This work introduces a new simulation approach to the evaluation of the time-domain electromagnetic (EM) field useful in the modeling of tapered waveguide for the Photonic Crystal Slab (PCS) coupling. Only solutions of two scalar Helmholtz-equations are used in the evaluation of electric and magnetic Hertzian-potentials that yields the EM field and the frequency response of the tapered waveguide. By considering simultaneously an analytical and a numerical approximation it is possible to reduce the computational burden. In order to compare the computational time we analyze the 2D structure by also using the Finite Difference Time Domain (FDTD) method and by the 3D Finite Element Method (FEM). The method is applied by starting from design criteria of the tapered structures in order to set the correct geometrical and physical parameters, and considers the field-perturbation effect in proximity of the dielectric discontinuities by generators modeling.

OCIS codes: (000.4430) Numerical approximation and analysis; (310.0310) Thin films.

References and links

1. K.S. Yee, "Numerical solution of initial boundary value problems involving maxwell's equation in isotropic media," IEEE Trans. Antennas Propagat. **AP-14**, 302-307 (1966).
2. W. J. R. Hoefer, "The transmission-line matrix method- Theory and applications," IEEE Trans. Microwave Theory Tech. **MTT-33**, 882-893 (1985).
3. M. Fujii, and W J. R. Hoefer, " A three-dimensional Haar-wavelet-based multiresolution analysis similar to the FDTD method-derivation and application, " IEEE Trans. Microwave Theory Tech. **46**, 2463-2475 (1998).
4. A. Massaro and T. Rozzi, "Rigorous time-domain analysis of dielectric optical waveguides using Hertzian potentials formulation," Opt. Express. **14**, 2027-2036 (2006).
5. A. Massaro, L. Pierantoni, and T. Rozzi , " Time-domain modeling and filtering behavior of guided-wave optics by Hertzian potentials," Proc. SPIE **6183** (2006).
6. M. Couture, "On the numerical solution of fields in cavities using the magnetic Hertz vector," IEEE Trans. Microwave Theory and Tech. **MTT-35**, 288-295 (1987).
7. K. I. Nikoskinen, "Time-domain study of arbitrary dipole in planar geometry with discontinuity in permittivity and permeability," IEEE Trans. Antennas Propag. **39**, 698-703 (1991).
8. T. Rozzi and M. Farina, *Advanced electromagnetic analysis of passive and active planar structures*, (IEE Electromagnetic wave series 46 , London. 1999), Ch.2.
9. C.G. Someda, *Onde elettromagnetiche* , (UTET Ed., Torino 1996), Ch. I.
10. N. Marcuvitz ,and J. Schwinger, "On the representation of the electric and magnetic field produced by currents and discontinuities in wave guides," J. Appl. Phys. **22**, 806-820 (1951).
11. N. C. Frateschi, A. Rubens, B. De Castro, " Perturbation theory for the wave equation and the effective refractive index approach," IEEE J. Quantum Electron. **QE-22**, 12-15 (1986).
12. A. Yariv, *Quantum Electronics*, (John Wiley & Sons , 3rd ed. Canada 1989), Ch. 22.
13. D.Marcuse, *Theory of Dielectric Opt. Waveguides*, (Academic Press, New York 1974), Ch. I.
14. A. Taflove, S. C. Hagness, *Computational Electrodynamic: the Finite-difference Time-domain Method*, (Arthec House Publishers, sec. ed., London 2000), Ch. 2,3,4,7.

#88268 - $15.00 USD Received 4 Oct 2007; revised 15 Nov 2007; accepted 19 Nov 2007; published 28 Nov 2007

15. G. Mur, "Absorbing boundary conditions for the finite-difference approximation of the time-domain electromagnetic field equations," IEEE Trans. Electromagnetic Compatibility **23**, 377-382 (1981).

1. Introduction

Time domain methods such as finite-difference time-domain (FDTD) [1], transmission line matrix (TLM) [2], and wavelet-Galerkin [3] methods are gaining importance by virtue of their versatility and the natural way in which they simulate what happens in reality and represent a powerful methods for solving electromagnetic problems. For high frequency optical structures the complexity of problems grows, and an high computer performance is requested. The rigorous Hertzian Potentials formulation can be used for simulation of full-wave propagation and reflection in the time domain, it is not time- and memory-intensive and is suitable for structure of large optical dimensions [4],[5] (in the 2D model we estimate an half reduction of the computational time respect to the 2D TLM method [5]). We propose an efficient numerical algorithm to solve the EM field behavior in a practical case of a coupling between a 3D tapered waveguide and photonic crystal slab (PCS) . This method considers the Hertz vectors[6]-[8] starting from the Helmholtz scalar equations [8]-[9] and the perturbed effect of the dielectric discontinuities [10]-[12] . The number of equations to solve are reduced to two scalar equations instead of six, subsequently all the EM components are obtained by the Hertzian potentials [6]-[8]. In the frequency domain the transmission and reflection properties of dielectric discontinuities (slanted dielectric profile of the tapered waveguide) may be derived by means of an equivalent circuit [10],[11],[12] that automatically ensures continuity of the fields and their first derivatives along the propagation-directions. If potentials are used, instead, second derivatives are involved and generators are necessary at each dielectric interface. The generators decrease the grid cell dimension and so the computational time with a good convergent solution. The method is developed by considering the design criteria of a tapered waveguide (see Fig. 1) that is coupled to a 2D PCS waveguide. As reported in Fig. 1 the tapered waveguide is directly connected to the guiding region of the PCS in order to transfer the maximum energy with high efficiency. The analytical model (used to reduce a 3D problems in 2D one through the effective index of the vertical structure), and the numerical Hertzian Potentials Method (HPM) model with generators (for solving the 2D problem) represent a good method for simulating complex 3D structures. We resume the analysis of this work in the following steps: i) analysis and design of tapered waveguide regarding to the PCS coupling in order to obtain a single TE mode at the PCS input (see Fig. 1) ; ii) time-domain Hertzian potentials modeling and computational time comparison between 2D Hertzian Potential Method (HPM), 2D FDTD method, and 3D FEM method. i) We define a modal map by using the dispersion-equations [13] in order to fix all the operative geometrical and optical parameters. Only a TE mode will propagate at the PCS input (single mode condition). ii) We use the effective refractive index evaluated along the z-direction (see Fig. 2) for a 2D modeling of the tapered waveguide (we solve a 3D problem in a 2D case) which proves the coupling and the E field confinement at the input and inside a PCS with air circular holes and guiding region; the results are compared with 2D FDTD and 3D FEM in order to verify the convergence of the solution and to evaluate the computational cost performance.

#88268 - $15.00 USD Received 4 Oct 2007; revised 15 Nov 2007; accepted 19 Nov 2007; published 28 Nov 2007

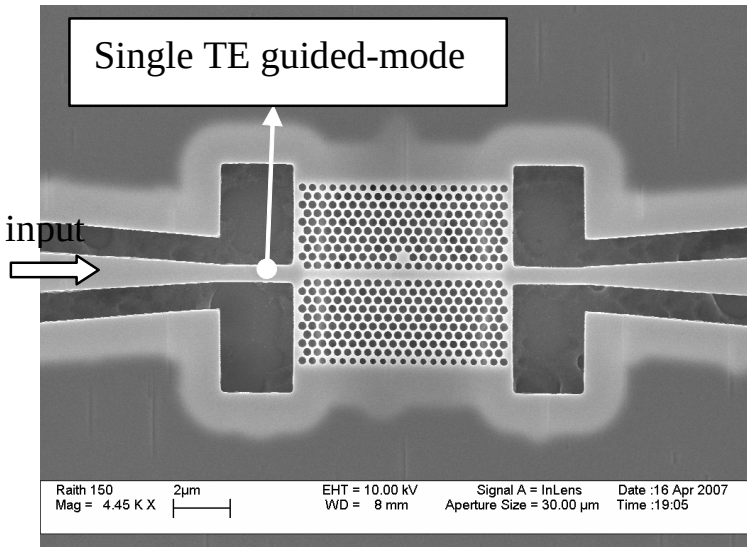

Fig. 1. SEM image of the fabricated photonic crystal with the tapered waveguide.

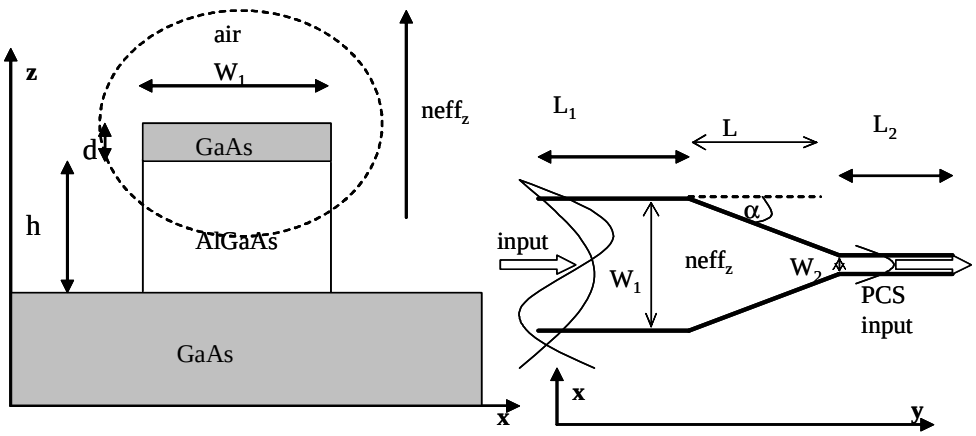

Fig. 2. Cross section of tapered waveguide and analytical approach (α=atan((W_1/2)-(W_2/2))/L).

#88268 - $15.00 USD Received 4 Oct 2007; revised 15 Nov 2007; accepted 19 Nov 2007; published 28 Nov 2007

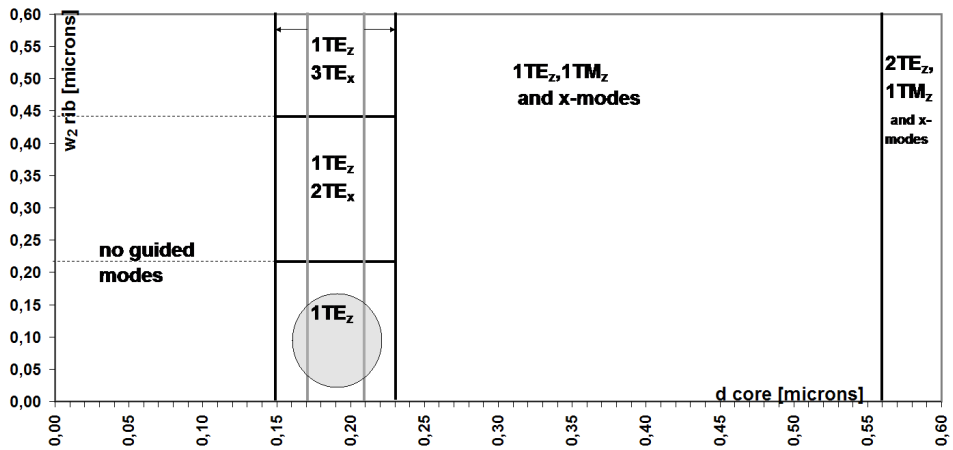

Fig. 3. Modal map by varying the thickness of the core d_{core} and width w_2. The working region is the single TEz mode-region (λ_0 =1.31µm, ncore(GaAs)=3.408).

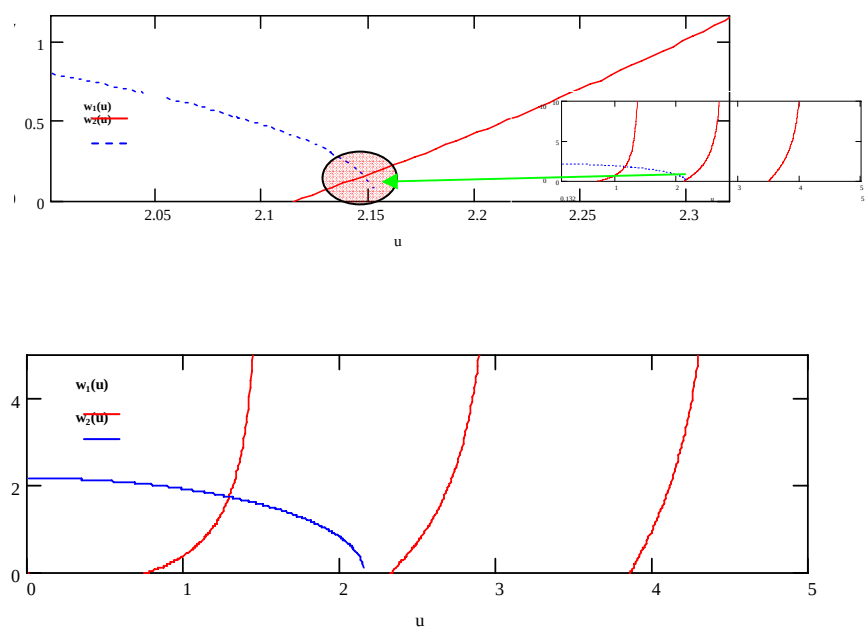

Fig. 4. Example of graphical approach of the dispersion equations solution (λ_0 =1.30µm, n_{core}(GaAs)=3.408 , n_{sub}(AlGaAs)=3.042, d_{core}=0.56µm + 20nm). TE dispersion equation (above), TM dispersion equation (below).

2. Analysis and design of tapered waveguide.

In order to define a modal region map (Fig. 3) we have considered the GaAs core refractive index n_{core}(GaAs)=3.408 at the working wavelength λ_0=1.31 µm (waveguide operation

#88268 - $15.00 USD Received 4 Oct 2007; revised 15 Nov 2007; accepted 19 Nov 2007; published 28 Nov 2007

wavelength). Figure 3 describes the modal region of the asymmetric slab waveguide and defines the geometrical parameters for a single mode condition. The analysis begins in the transverse z-direction in order to define the effective refractive n_{effz} index. The dispersion equations [13] are used for a graphical analysis of the single mode region that is useful to evaluate the sensitivity of the solution near the frequency cut-off (of the single TE guided condition) by changing the core thickness. We show in Fig. 4 an example of frequency-cut graphical evaluation concerning the TE and the TM analysis. The used dispersion-equations are [13]

$$w_1(u) = \frac{(u^2 \tan(2u) - u\sqrt{\mathrm{v}_1^{\,2} - u^2})}{u + \tan(2u) \cdot \sqrt{\mathrm{v}_1^{\,2} - u^2}} \tag{1}$$

for the TE modes, and

$$w_1(u) = \frac{(u^2 \varepsilon_1 \varepsilon_3 \tan(2u) - u\varepsilon_2 \varepsilon_3 \sqrt{\mathrm{v}_1^{\,2} - u^2})}{u\varepsilon_1 \varepsilon_3 + \varepsilon_2^2 \tan(2u) \cdot \sqrt{\mathrm{v}_1^{\,2} - u^2}} \tag{2}$$

for the TM modes, with

$$\begin{aligned} \mathrm{v}_1 &= k_0 d_{core} \sqrt{\varepsilon_2 - \varepsilon_1} \\ \mathrm{v}_3 &= k_0 d_{core} \sqrt{\varepsilon_2 - \varepsilon_3} \\ w_2(u) &= \sqrt{\mathrm{v}_3^2 - u^2} \\ k_0 &= \omega \sqrt{\varepsilon_0 \mu_0} \end{aligned} \tag{3}$$

and ε_1=1(air), ε_2=11.56(GaAs), ε_3=10.89(AlGaAs), k_0 is the wave number in the free space. By using (1),(2),(3) we evaluate $k_z=u/d_{core}$ and then effective index in the z-direction ε_{effz} by the wavenumber conservation equation

$$k_0^2 \varepsilon_{effz} = k_0^2 \varepsilon_2 - k_z^2 \tag{4}$$

With the help of map shown in Fig. 3 we derived the core-thickness d_{core} and the width w_2 (see Fig. 2) in order to obtain only one TE propagated-mode at the PCS input. In Fig. 3 we show the working region in which only TE_z mode (only a propagation constant k_z will be solution of the dispersion equation) will propagates in the waveguide. In this map is also reported a security region (in to gray lines) by considering also a real possible error of ±20nm in the core thickness fabrication. In our case the single TE_z propagated modes is obtained by d_{core}=0.19 μm (n_{effz}=3.067 is the corresponding effective refractive index), w_2=0.22 μm.
After the z analysis we use the refractive n_{effz} in the x-y plane in order to analyze the behavior of the tapered waveguide by different α slanted-angles, and L lengths, by the time-domain Hertzian formulation [4]-[5] reported in the next section.

3. Time-domain Hertzian potentials modeling of tapered waveguide.

In Fig. 5 is shown the time-domain Hertzian Potentials algorithm used in this work[4]-[5]

#88268 - $15.00 USD Received 4 Oct 2007; revised 15 Nov 2007; accepted 19 Nov 2007; published 28 Nov 2007

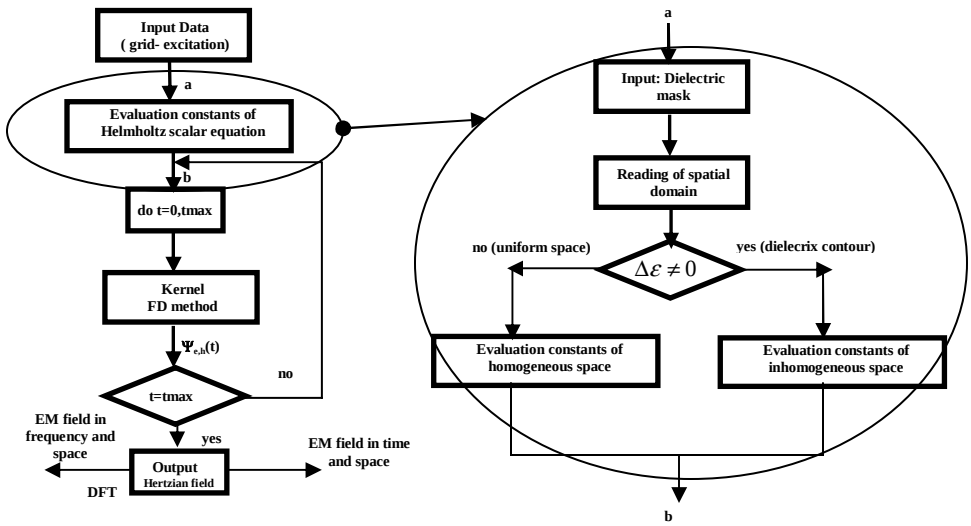

Fig. 5. Finite difference time-domain Hertzian potentials algorithm.

The Hertzian electric and magnetic vectors are [6]-[8] in rectangular coordinates represented by

$$\overline{\Pi}_e = \mathbf{a}\psi_e(x,y,z,t)$$
$$\overline{\Pi}_h = \mathbf{a}\psi_h(x,y,z,t) \tag{1}$$

where **a** is unit vector. From (1) it is possible to evaluate all the components of the EM field as

$$\overline{\mathbf{E}} = \nabla\nabla\cdot\overline{\Pi}_e - \varepsilon\mu\frac{\partial^2}{\partial t^2}\overline{\Pi}_e - \mu\frac{\partial}{\partial t}(\nabla\times\overline{\Pi}_h)$$
$$\overline{\mathbf{H}} = \nabla\nabla\cdot\overline{\Pi}_h - \varepsilon\mu\frac{\partial^2}{\partial t^2}\overline{\Pi}_h + \varepsilon\frac{\partial}{\partial t}(\nabla\times\overline{\Pi}_e) \tag{2}$$

$\Psi^{e,h}(x,y,z,t)$ represents the solution of the homogeneous wave equation for a non-dissipative medium [4]

$$\nabla^2\psi_{e,h}(x,y,z,t) - \mu\varepsilon\frac{\partial^2\psi_{e,h}(x,y,z,t)}{\partial t^2} = 0 \tag{5}$$

It is known that the scalar wave equation may lead to inconsistencies because, in an inhomogeneous medium, it is, in general, not equivalent to Maxwell's equations. Electromagnetic scattering problems, including free space, involve the calculation of the fields produced in the presence of geometrical discontinuities by arbitrary currents. Such discontinuities may be replaced by equivalent generators [4], (see Fig. 6(a) and Fig. 7), giving an accurate solution of the EM field for structures with high dielectric contrast. In fact the scalar wave equation (5) for a non-dissipative medium can be rewritten as [4]

$$\nabla^2\Psi_{e,h}(x,y,z,t) - \mu\varepsilon\frac{\partial^2\Psi_{e,h}(x,y,z,t)}{\partial t^2} - \mu\frac{\partial^2 P_{pert}(x,y,z,t)}{\partial t^2} = 0 \tag{6}$$

#88268 - $15.00 USD Received 4 Oct 2007; revised 15 Nov 2007; accepted 19 Nov 2007; published 28 Nov 2007

where

$$\mathrm{P(x,y,z,t)} = \Delta\varepsilon(x, y, z,\mathrm{t})\Psi_{\mathrm{e,h}}(x, y, z,\mathrm{t}) \tag{7}$$

represents the dielectric polarization and for the bi-dimensional case:

$$\Delta\varepsilon = \varepsilon_{i+1} - \varepsilon_i \quad i = cell\ position \text{ in x direction .} \tag{8}$$

$$\Delta\varepsilon = \varepsilon_{j+1} - \varepsilon_j \quad \mathrm{j} = cell\ position \text{ in y direction .} \tag{9}$$

Therefore we solve (6) in proximity of the dielectric interfaces, and (5) in the homogenous region. The difference between the parametric solution of (5), and (6) in the iterative form (by using the finite difference FD discretisation [14]),is in the coefficients [4]; in fact for one propagation direction

$$\psi^{n+1}(j) = \psi^n(j+1)\left(\frac{b}{a}\right) + \psi^n(j)\left(\frac{2a-2b}{a}\right) + \psi^{n-1}(j)(-1) + \psi^n(j-1)\left(\frac{b}{a}\right) \tag{10}$$

$$\psi^{n+1}(j) = \psi^n(j+1)\left(\frac{b}{a'}\right) + \psi^n(j)\left(\frac{2a'-2b}{a'}\right) + \psi^{n-1}(j)(-1) + \psi^n(j-1)\left(\frac{b}{a'}\right) \tag{11}$$

with

$$\begin{aligned} a &= \frac{\mu\varepsilon}{(\Delta t)^2} \\ a' &= a + \frac{\mu\Delta\varepsilon}{(\Delta t)^2} \\ b &= \frac{1}{(\Delta z)^2} \end{aligned} \tag{12}$$

#88268 - $15.00 USD Received 4 Oct 2007; revised 15 Nov 2007; accepted 19 Nov 2007; published 28 Nov 2007

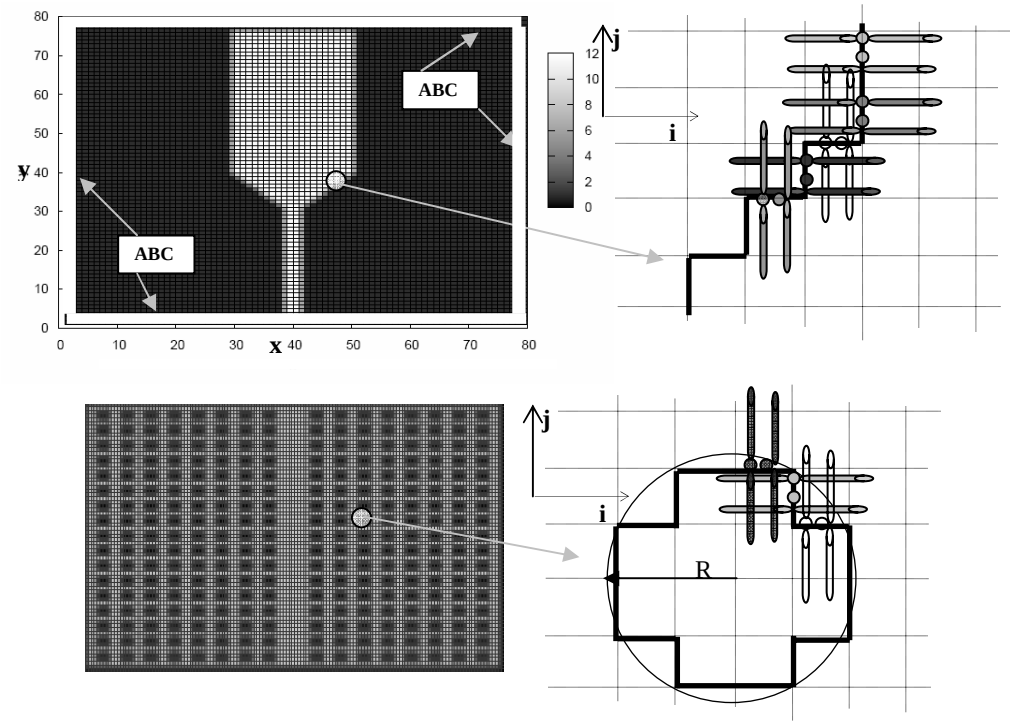

Fig. 6. (a). Above :computational domain Ω=(x,y) and dielectric grid-mask of 45 degree tapered profile with transmission line perturbed modeling; below: PCS with guiding region and perturbed modeling of air hole (radius R).

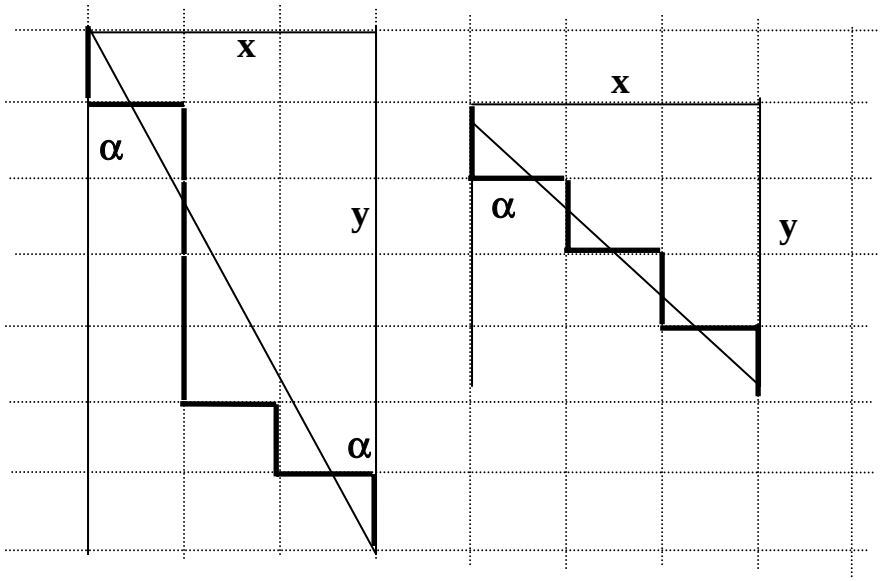

Fig. 6. (b). Left: geometrical construction of the unit cell of dielectric tapered profile (α=atan(x/y)=18.449 deg) ; right: slanted angle of 45 deg.

#88268 - $15.00 USD Received 4 Oct 2007; revised 15 Nov 2007; accepted 19 Nov 2007; published 28 Nov 2007

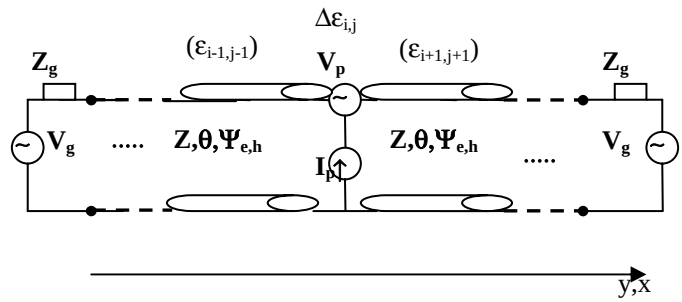

Fig. 7. Transmission line modeling of dielectric profile.

In Fig. 6(a), Fig. 6(b) and Fig. 7 we show the discretisation and the modeling of the dielectric profiles (dielectric tapered profile and circular air hole profile). The algorithm define the sub-domain boundaries (profiles) by inserting the generators around a reference cell when the perturbed conditions (8) and (9) are satisfied. We observe that the generators V_P and I_P of Fig.7 represent the variation of the coefficients (12), and the dielectric mask is loaded as a bidimensional vector of the x-y spatial domain , so it is possible to define the perturbed region (inhomogeneous region) by considering all the cells around the reference cell. The flow chart of this procedure is reported in Fig. 4. Therefore we solve (6) in proximity of the dielectric interfaces (inhomogeneous region) , and (5) in the uniform space (homogenous region) by considering the different parametric solutions given by (12). The absorbing boundary conditions (ABCs) [5],[14],[15], around the computational domain Ω=(x,y) (see Fig. 6), permits all outward-propagating numerical waves to exit Ω as if the simulation were performed on a computational domain of infinite extent. Extremely small local reflection coefficient of the order of 10^{-11} is attained in the simulations. In the 2D case the matrix structure that considers the spatial domain and the ABCs is

$$\downarrow\rightarrow \text{ i,j space domain position} \qquad (13)$$

$$\begin{pmatrix} ABC & ABC & ABC & ABC & ABC & ABC & ABC & ABC & ABC \\ ABC & \cdot & \cdot & \psi^n(i,j) & \psi^n(i+1,j) & \psi^n(i+2,j) & \cdot & \cdot & ABC \\ ABC & \cdot & \cdot & \cdot & \psi^n(i+1,j+1) & \cdot & \cdot & \psi^n(m,j+1) & ABC \\ ABC & \cdot & \cdot & \cdot & \cdot & \cdot & \cdot & \cdot & ABC \\ ABC & \cdot & \cdot & \cdot & \psi^n(i+1,l) & \cdot & \cdot & \cdot & ABC \\ ABC & ABC & ABC & ABC & ABC & ABC & ABC & ABC & ABC \end{pmatrix}^{m \times l}$$

where *m* x *l* is the node number of the spatial domain , and time-step is fixed. By approximation (10),(11),(12) a small node number is requested for the numerical convergence.

4. Time-domain Hertzian potentials results.

As shown in Fig. 8 (source time-evolution) the source is decomposed in two components ψ_e and ψ_h that construct the wavefront in the spatial domain (x,y). We use in both directions the source as a carrier modulated by an exponential signal:

$$\Psi^{e,h}_{source} = \exp(-(t \cdot dt / T_0)^2) \cdot \cos(\omega \cdot t \cdot dt) \qquad (13)$$

where ω is the angular frequency referred to an operative wavelength λ_0=1.31μm, T_0 is a constant, and *dt* is the time step. Figure 9 proves that a tapered waveguide with w_1=5.94μm, w_2=0.22μm ,α=30 deg., after some time-steps, guides the single TE mode at the PCS input

#88268 - $15.00 USD Received 4 Oct 2007; revised 15 Nov 2007; accepted 19 Nov 2007; published 28 Nov 2007

(the parameters used in the simulation are: $dx=dy=0.11*10^{-7}$m., $dt=$ $3.67*10^{-16}$sec., $\lambda_0=1.31\mu$m, $T_0=$ $8*10^{-15}$sec.) . A spatial monitoring of the E_z field is reported in Fig. 10: we fix the time-step and evaluate the spatial E_z profile for different cross-sections. Also in this case is possible to evaluate the coupled-field inside the structure and the radiated field in air (the field confined inside the waveguide is about one order higher than the radiated field) . For the simulation of Fig.10 we set $w_1=5.94\mu$m, $w_2=0.22\mu$m and $\alpha=14$ deg.
The evaluation of transmission coefficient completes the analysis of the tapered waveguides.
In order to define the frequency response we consider the Discrete Fourier Transform (DFT). The scattering parameters *Sm,n* can be obtained for an impulsive excitation as follows [14]

$$S_{m,n}(\omega, y_m, y_n) = \frac{\hat{E}_m(\omega, y_m)}{\hat{E}_n(\omega, y_n)} \sqrt{\frac{Z_{0,n}(\omega)}{Z_{0,n}(\omega)}} \tag{14}$$

where $\hat{E}_m$ is the phasor voltage (DFT of E_z component) at the port *m* at observation plane y_m; $\hat{E}_n$ is the phasor voltage at the port *n* at observation plane y_n ; and $Z_{0,m}$ and $Z_{0,n}$ are the characteristic impedances of the line connected to these ports defined as

$$Z_0(\omega, y_i) = DFT(E_z, y_i) / DFT(H_x, y_i). \tag{15}$$

Figure 11 and Fig. 12 show the scattering transmission coefficient $S_{ba}=S_{21}$ with the port 1 and port 2 defined by the references line a=y_1 and b=y_2 respectively: the tapered waveguide with $w_1=5.94\mu$m, $w_2=0.22\mu$m and $\alpha=14$ deg, and 45 deg. is characterized by an high transmission coefficient around the working wavelength $\lambda_0=1.31\mu$m. In particular in Fig. 11 we show the comparison between the frequency response of: a tapered waveguide with dx=dy=0.11μm with generators, of a tapered waveguide with dx=dy=0.05μm without generators, and of a 3D tapered waveguide with tetrahedron length of 0.01μm (FEM simulation). We observe that the solution with dx=dy=0.05μm is characterized by a numerical error oscillations (absence of generators). It is evident by the graph that the solution with dx=dy=0.11μm (with generators) converges better without oscillations. In order to verify the convergence solution we show in the same graph the 3D FEM solution. Moreover in Fig. 12 is reported the convergence between the S_{21} Hertzian potentials coefficient and the 2D FDTD one: HPM results converge with greater unit cell grid dimension as compared to the FDTD method (in FDTD with dx=dy=0.01μm, instead in HPM by using dx=dy=0.11μm). In order to observe the coupling effect on a PC structure we simulate the whole structure (PC slab with a guide coupled to a tapered waveguide). This kind of PC (with a guiding region) is important because it is possible to increase the quality Q-factor of the whole structure. After about 400 time-steps the PCS will couple with the waveguide with width w_2. By the single mode condition the maximum energy will be transmitted to the PC that will generate PC modes characterized by the group velocity defined by the geometry of the crystal. In this simulation we analyze the coupling at the PC input by observing also the propagation inside a PC structure in order to confirm the presence of the field in the PC guiding region. We consider in our numerical example air holes with radius R=0.11μm in an effective medium with $n_{effz}=3.067$; the x-period is 3*R, the y-period is 2,5*R , and w_2 is the width of the guiding region. We show in Fig.13 the time evolution of the E_z field component inside the PCS by proving the efficacy of the tapered waveguide in terms of field confinement. We also evaluate the coupling efficiency at the PC input by :

#88268 - $15.00 USD Received 4 Oct 2007; revised 15 Nov 2007; accepted 19 Nov 2007; published 28 Nov 2007

$$\eta = \frac{W_{output}(y;t)}{W_{input}(y;t)} = \frac{\int_{w_1}^{w_2} P_y(x,y,t)dx}{\int_{w_1}^{w_2} P_y(x,y,t)dx} = \frac{\int_{w_1}^{w_2} (E_x H_z + (-E_z H_x))dx}{\int_{w_1}^{w_2} (E_x H_z + (-E_z H_x))dx} \tag{16}$$

where P_y represents the Poynting vector along the y propagation direction. Figure 14 shows how the efficiency decreases when the α-angle increases. For large α values most energy will be irradiate in the air region. By comparing Fig. 12 with Fig.14 it is evident that at working wavelength of λ_0=1.31 μm the transmission is high α=14 deg. and α=45 deg. , but a good coupling efficiency is performed by a tapered waveguide with α=14 deg. The results is validated also by Fig. 10 in which , for α=14 deg., the EM field is well confined at the output of the tapered waveguide.

We validate the model presented in this work (analytical model by using effective index and numerical generators model) by comparing the Central Processing Unit (CPU) time for different numerical methods. The computation time comparison is reported in the Table I for different tapered waveguides with L_1=L_2=5 μm (see Fig.2), and for a 1-GHz PC, 512/M-RAM. In this comparison we consider the 2D FDTD method (with effective index approach and dx=dy=0.01μm), and the 3D FEM method. In order to compare the 2D Hertzian Potentials solution with the 3D FEM one, we refine the length of tetrahedral elements (FEM mesh) below the specified value of 0.01 μm . The length of a tetrahedron is defined as the length of its longest edge. In the Hertzian Potential method all the field components depend only on the $\Psi^{e,h}$ scalar potentials [4], instead in the FDTD algorithm the components are interrelated and so the computational cost increases.

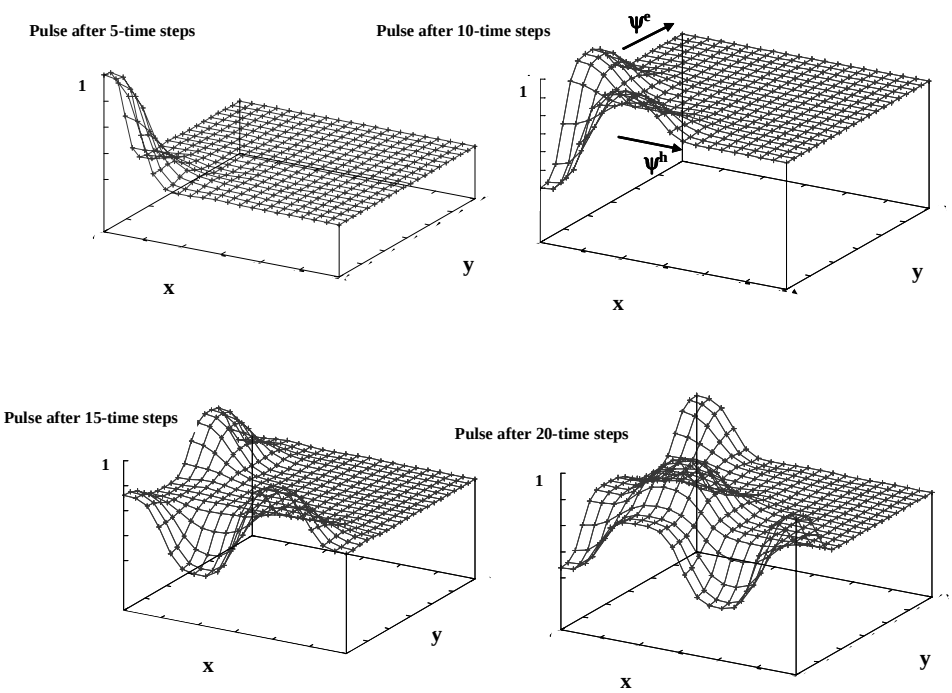

Fig. 8. Source: time-evolution in air (pulse excitation).

#88268 - $15.00 USD Received 4 Oct 2007; revised 15 Nov 2007; accepted 19 Nov 2007; published 28 Nov 2007

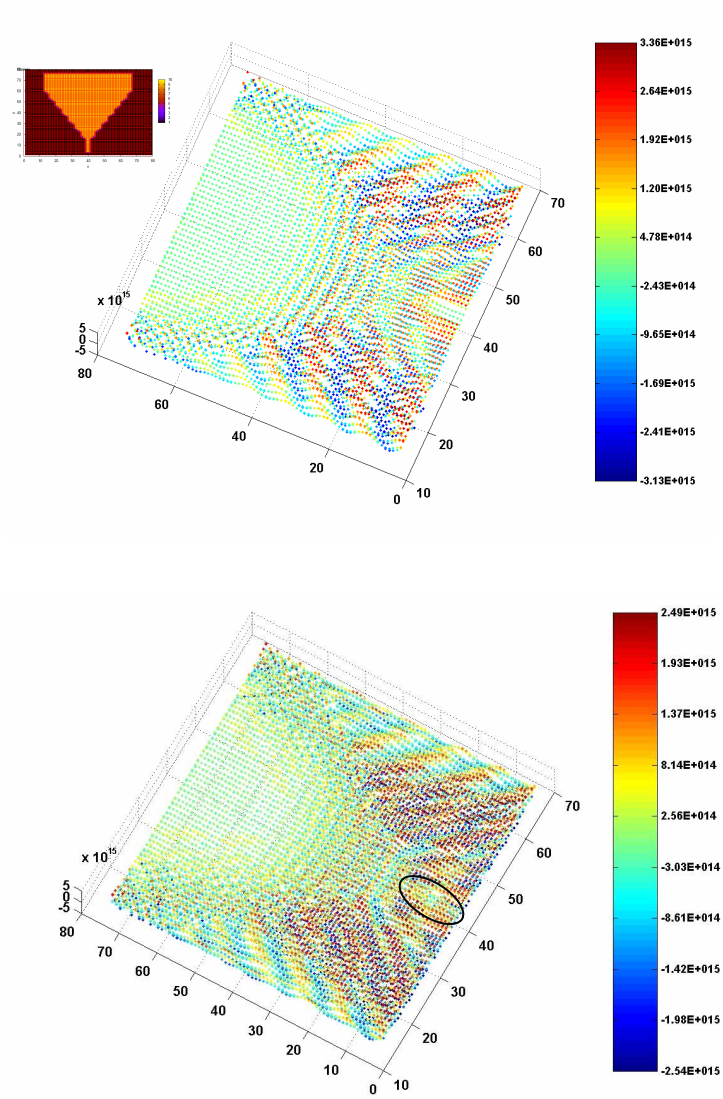

Fig. 9. Time evolution of Ez components after 350 and 400 time-steps in spatial domain (x,y). After 400 time steps the field is coupled in the guide with thickness w_2).

#88268 - $15.00 USD Received 4 Oct 2007; revised 15 Nov 2007; accepted 19 Nov 2007; published 28 Nov 2007

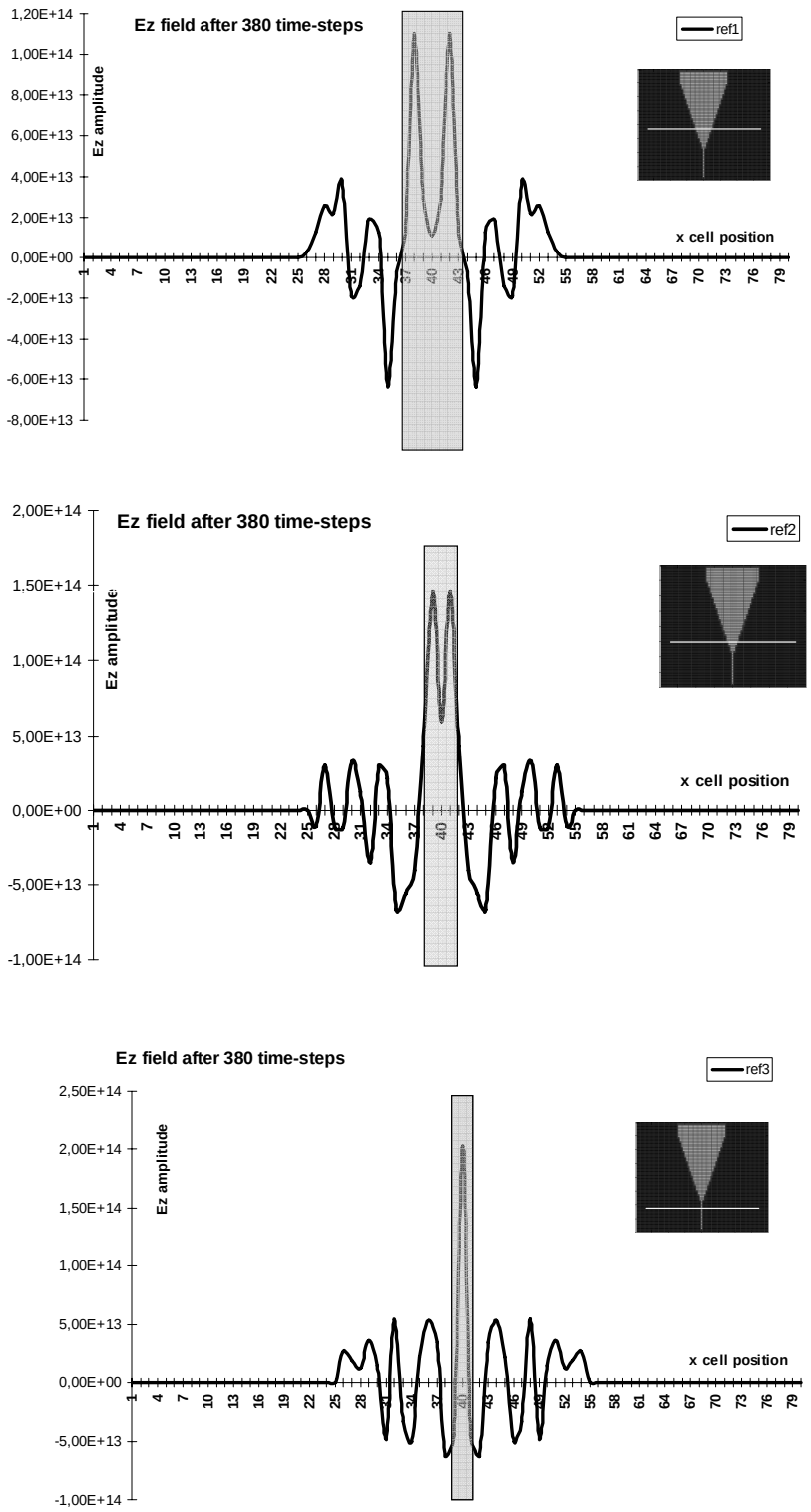

Fig. 10. Ez field component after 380 time-steps for different cross-section (reference of y-position).

#88268 - $15.00 USD Received 4 Oct 2007; revised 15 Nov 2007; accepted 19 Nov 2007; published 28 Nov 2007

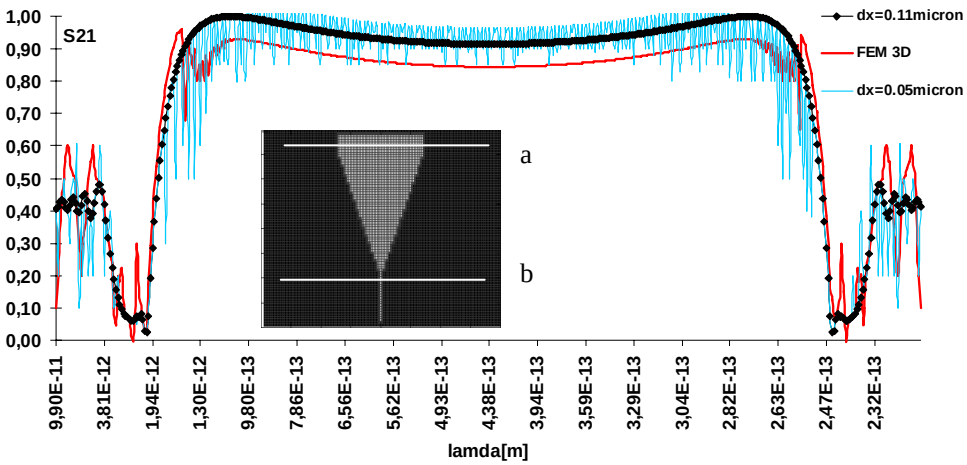

Fig. 11. Frequency responses of a tapered waveguide with w_1= 5.94µm, w_2=0.22µm ,α=14 deg; a and b are the reference section of the S_{21} transmission coefficient.

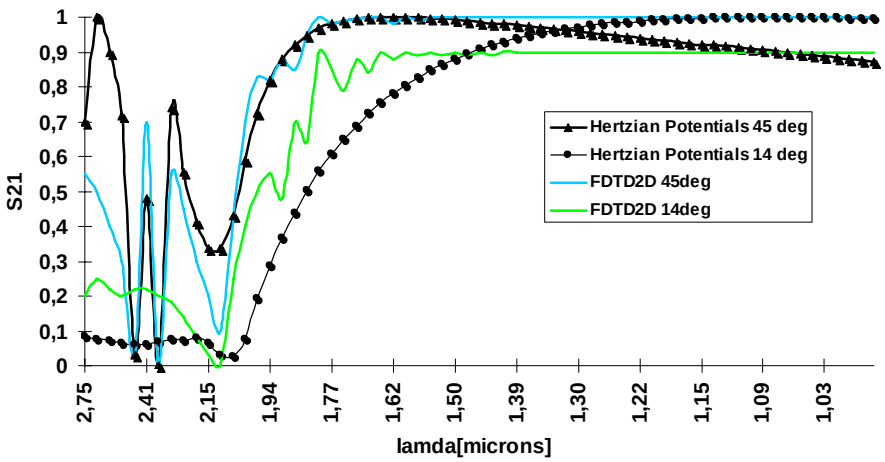

Fig. 12. FDTD and Hertzian Potentials S_{21} transmission coefficient of a tapered waveguide with w_1= 5.94µm, w_2=0.22µm, α=14 deg., α=45 deg.

#88268 - $15.00 USD Received 4 Oct 2007; revised 15 Nov 2007; accepted 19 Nov 2007; published 28 Nov 2007

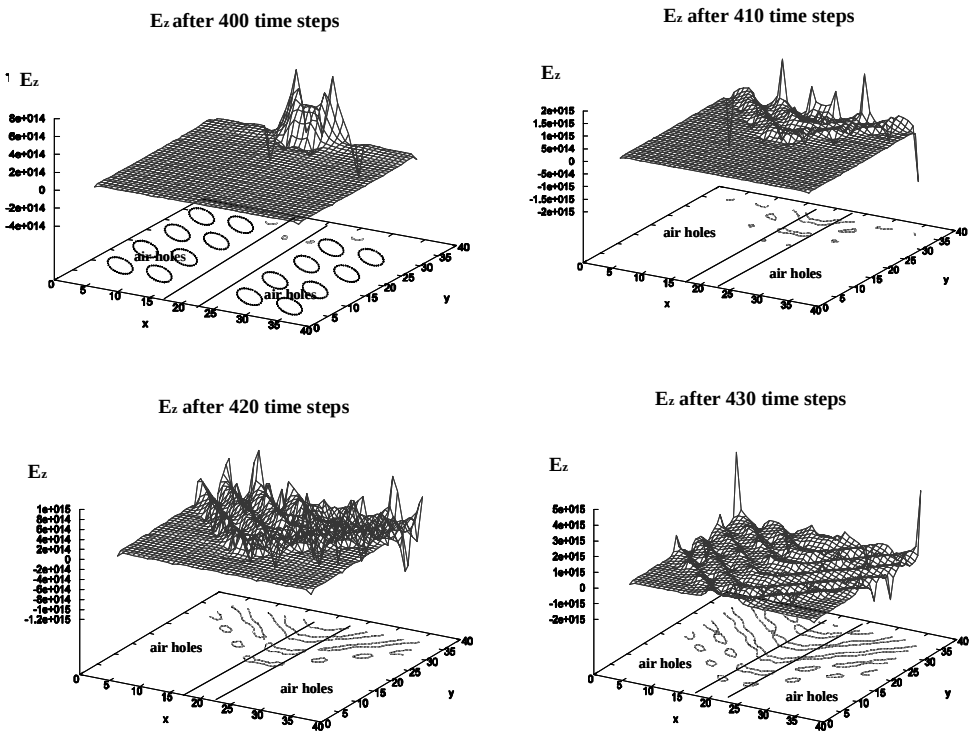

Fig. 13. Time evolution of E_z field component after 400, 410, 420, and 430 time-steps inside the PC after the coupling with the tapered waveguide (with thickness w_2). After about 400 time-steps the wave arrives at the PCS input.

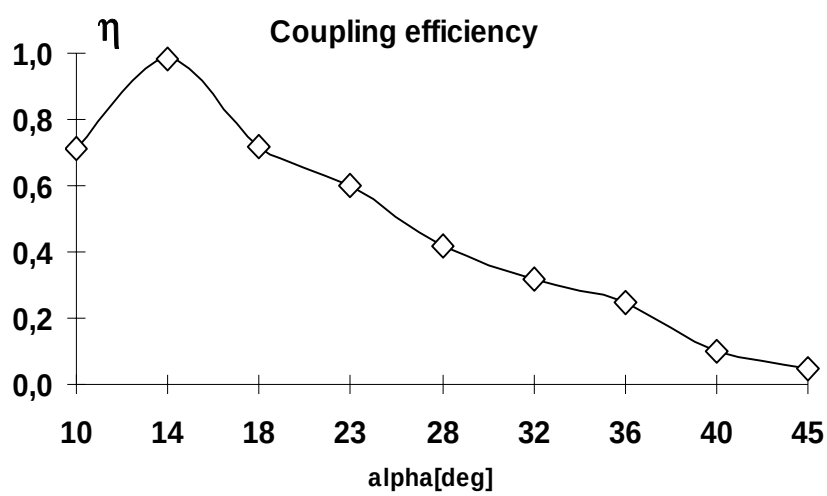

Fig. 14. Coupling efficiency for different alpha angles.

#88268 - $15.00 USD Received 4 Oct 2007; revised 15 Nov 2007; accepted 19 Nov 2007; published 28 Nov 2007

Table I. Comparison between CPU time for the 2D Hertzian Potenzials Method (HPM) , FDTD 2D , and 3D FEM method.

α [deg]	**L [μm]**	**CPU time 2D HPM [sec.]**	**CPU time 2D FDTD [sec.]**	**CPU time 3D FEM [min]**
10	16.22	2.3	4.8	45
14	11.47	1.9	4.3	42
18	8.80	1.6	3.5	39
23	6.73	1.3	2.9	38
28	5.38	1.2	2.6	36
32	4.57	1.0	2.4	33
36	3.93	0.9	2.1	31
40	3.40	0.8	1.9	29
45	2.86	0.7	1.6	25

5. Conclusion

This Hertzian potentials formulation with effective refractive index approach provides the 3D behavior of the tapered waveguide with a low computational cost and a good numerical convergence solution. The numerical model shows the field confinement and field PCS-coupling for different slanted α angles at the working wavelength of λ_0=1.31 μm. The proposed time-domain model is used to evaluate the single TE transmitted field at the PCS input by considering waveguide coupling, and the frequency response around the working wavelength. We complete the coupling analysis by comparing the method with the 2 FDTD and 3D FEM results, and by evaluating the field coupled inside the PCS along the guiding region. The numerical and the analytical approximations used in this work give the same convergent results of the 3D FEM model with less computational cost.

#88268 - $15.00 USD Received 4 Oct 2007; revised 15 Nov 2007; accepted 19 Nov 2007; published 28 Nov 2007